A case study on optimum tip speed ratio and pitch angle laws for wind turbine rotors operating in yawed conditions

A case study on optimum tip speed ratio and pitch angle laws for wind turbine rotors operating in yawed conditions

A Cuerva-Tejero[1], O Lopez-Garcia[1], D Marangoni[2], F González-Meruelo[1]

[1] Instituto Universitario de Microgravedad Ignacio Da Riva, E.T.S.I.Aeronáuticos, Universidad Politécnica de Madrid, E-28040 Madrid, Spain
[2] Mechanical Engineering Department, University of Padova, I-35131, Padova, Italy

E-mail: `alvaro.cuerva@upm.es`

Abstract.
    The values of the tip speed ratio and blade pitch angle that yield maximum power coefficient are calculated for a rotor operating in yawed conditions. In a first step, the power coefficient is determined using a model based on the blade element momentum theory (BEMT) which includes a Prandtl-Glauert root-tip losses correction, a non-uniform model for the axial and tangential induction factors, and a model of the rotational augmentation effects. The BEMT model is validated with the experimental data from the NREL-UAE. The maximum values of the power coefficient are determined for different yaw angles and the corresponding values of the tip speed ratio and blade control angle are obtained. The maximum power coefficient using these optimum laws is compared to the maximum power coefficient using the optimum laws of the non-yawed case and it is shown that there is a gain in the power coefficient. For the case study presented in this paper it has been found that for yaw angles of 30° about 10% of the power coefficient can be recovered.

1. Introduction
Optimisation of energy production of wind turbines plays a crucial role in the development of such a technology nowadays, and researchers are used to explore new control strategies to improve the efficiency of the machines. As it is well known, the yaw control of wind turbines is crucial since the situation where a machine is operating in yawed conditions is quite frequent and it gives rise to a high reduction of the power coefficient and to a remarkable loading increment. Most of the times the yawed condition occurs because the wind direction changes and the yaw control of the wind turbine cannot follow these changes due to the large characteristic times of the yaw dynamics, the need to keep gyroscopic loads bellow certain level and the limitations of the yaw motors. Wind turbine manufacturers normally introduce delays in the yaw control laws of the machines. The objective of these delays is to make sure that the rotor begins to be oriented only after a new wind direction is stabilised for some time.

    The main idea behind this paper is to quantify up to which extend the tip speed ratio and the control angle of the NREL-UAE blade that produce maximum power coefficient depend on the yaw angle. The control of optimum rotational speed depending on the yaw angle could open

a way to increase the production during the short frequent periods when the rotor is yawed, since the dynamic of the generator and pitch is much faster than the yaw one.

There are very few data sets (from computational or real test) published describing the dependence, with enough resolution, of the power coefficient, C_P, on the tip speed ratio, λ, being $\lambda = \Omega R U_\infty^{-1}$ (Ω is the rotational speed, R is the rotor radius and U_∞ is the free wind speed), the control angle of the blade, θ_C, and the yaw angle Φ. A BEMT model in yaw was presented in [1] and surface $C_P(\lambda, \Phi)$ is computed showing that increasing yaw angle the optimum tip speed ratio at which the power coefficient is attained decreases. In [2], also reproduced in [3], a surface $C_P(\lambda, \Phi)$ is presented. Divalentín´s results show that the value of λ producing maximum C_P decreases as Φ increases (from $\lambda_{\rm op} \simeq 8.25$ for $\Phi = 0°$ down to $\lambda_{\rm op} \simeq 5$ for $\Phi = 5°$). In [4] a surface $C_P(\lambda, \Phi)$ for a wind turbine operated in a wind tunnel at constant blade control angle is presented. The results presented in [4] reveal that, in that case, the value of $\lambda_{\rm op}$ does not change with the yaw angle, at least with the experimental resolution applied (one experimental point every unit of λ). [5] computes $C_P(\lambda, \Phi)$ using a free wake vortex method for the Tjaereborg wind turbine. The curves show that the maximum power coefficient is reached for a tip speed ratio $\lambda_{\rm op} \simeq 8$. However, the power coefficient curve at this value of λ is so flat that it is difficult to know if the value of $\lambda_{\rm op}$ increases or decreases as the yaw angle increases.

The intention of the authors is to present this work in the most honest possible way. The authors know that these results could be controversial, most probably they are blade dependent, and even there is a possibility that the results could be a spurious output of the BEMT model associated with its level of uncertainty, since the obtained variations required for $\lambda_{\rm op}$ (one unit) and $\theta_{C\rm op}$ (1.5°) are small. However the authors consider that the validation of these results using more advanced computational methods or wind tunnel testing with high resolution in λ and θ_C would be clarifying in all aspects.

The paper is organised as follows. In section 2 the key details of the applied model based in the Blade Element Momentum Theory (BEMT) for the yawed rotor is presented. In order to validate the model, numerical results are compared to the experimental data in section 3, using the data set of the two bladed wind turbine tested at the NREL-UAE, see [6] for more information. In section 4 the power coefficient $C_P(\lambda, \theta_C; \Phi)$ of the NREL-UAE wind turbine is calculated. The maximum values of the surface $C_P(\lambda, \theta_C; \Phi)$ are determined for different yaw angles Φ, giving rise to the values $\lambda_{\rm op}(\Phi)$ and $\theta_{C\rm op}(\Phi)$ that maximise C_P for each Φ. Conclusions are presented in section 5.

2. Description of the model
To describe the aerodynamics of the wind turbine operating in yawed conditions a classical BEMT model following the Sharpe formulation (see [7]) is used together with a model to take into account rotational augmentation effects (see [8]).

2.1. Blade Element and Momentum Theory
The BEMT implements an aerodynamic induced velocity field at the rotor disk which is described by the axial and tangential induced velocity factors, a and a'. The axial induced velocity factor is non-uniform over the blade length and shows a dependence on the blade azimuth, ψ, and on the dimensionless radial position, $x = r\, R^{-1}$, that is $a(x, \psi)$, see [9] for a review of non-uniform inflow models. The tangential induced velocity factor a' is non-uniform over the blade length, $a'(x)$. As it is well-know, there exists a non-uniform component of the axial induced velocity factor which leads to an increment of the induced velocity at the rear end of the rotor disc and to a decrement at the forward end. For a yawed rotor the axial induced velocity can be expressed as

$$a(x, \psi) = a_0(x)\,(1 + K\,x\,\sin\psi)\,, \tag{1}$$

where a_0 the azimuth average value of the induced velocity factor and, the constant K, following [10], can be expressed by $K = \tan(\chi/2)$ where χ is the skewed wake angle, which is

$$\chi = \arctan\left(\frac{\sin\Phi}{\cos\Phi - a_0}\right).$$

The approach followed herein is to apply the classical momentum theory to a differential annular ring in order to determine the radial distributions of azimuthal averaged induced velocity factors, $a_0(x)$ and $a_0'(x)$. The blade element theory is applied, as usual, by defining the local inflow and computing the thrust and aerodynamic torque from the lift and drag coefficients of the corresponding blade section. For the yawed rotor, thrust and torque are functions of the blade azimuth position, ψ. Therefore, thrust and torque should be integrated along the differential annular ring in order to obtain their averaged values. The averaged induced velocities are modified using a Prandtl-Glauert correction to include root-tip losses, see for instance [11].

The BEMT model is based on equating the first two equations that establish that the differential thrust and torque predicted by the momentum theory, and the azimuthally averaged blade element equations should be equal, see [12]. The last equation is the definition of the root-tip loss factor. The equality of differential thrust is

$$8\,x\,a_0\left(\cos\Phi - a_0\right) = \frac{1}{2\pi}\int_0^{2\pi}\frac{\mathrm{d}C_T(x,\psi)}{\mathrm{d}x}\mathrm{d}\psi, \tag{2}$$

where the differential thrust, $\mathrm{d}C_T/\mathrm{d}x$, is written down

$$\frac{\mathrm{d}C_T}{\mathrm{d}x} = \sigma\left[\frac{U_R(x,\psi)}{U_\infty}\right]^2\left[c_{l,3D}(\alpha)\cos\phi(x,\psi) + c_{d,3D}(\alpha)\sin\phi(x,\psi)\right],$$

where σ is the rotor solidity, $c_{l,3D}$ and $c_{d,3D}$ the lift and drag coefficients corrected to account for rotational augmentation effects, see below, α the angle of attack which is $\alpha = \phi - \theta$, being $\theta = \theta_t + \theta_C$ with θ_t the blade twist and θ_C the pitch angle, U_R the resultant flow velocity at the blade element defined by

$$U_R(x,\psi) = U_\infty\left\{\left(\cos\Phi - \frac{a_0}{f}\right)^2 + \left[\cos\psi\sin\Phi + \lambda x\left(1 + \frac{a_0'}{f}\right)\right]^2\right\}^{1/2},$$

and ϕ the inflow angle which can be expressed by

$$\phi(x,\psi) = \arctan\left[\frac{\cos\Phi - \dfrac{a_0}{f}}{\cos\psi\sin\Phi + \lambda x\left(1 + \dfrac{a_0'}{f}\right)}\right],$$

where f is the root-tip loss factor.

Equating the differential torque computed by the momentum theory with the differential torque predicted by the blade element gives

$$8\lambda x^3 a_0'\left(\cos\Phi - a_0\right) = \frac{1}{2\pi}\int_0^{2\pi}\frac{\mathrm{d}C_Q}{\mathrm{d}x}\mathrm{d}\psi, \tag{3}$$

where the differential torque $\mathrm{d}C_Q/\mathrm{d}x$ predicted by the blade element theory can be expressed by

$$\frac{\mathrm{d}C_Q}{\mathrm{d}x} = \sigma x\left[\frac{U_R(x,\psi)}{U_\infty}\right]^2\left[c_{l,3D}(\alpha)\sin\phi(x,\psi) - c_{d,3D}(\alpha)\cos\phi(x,\psi)\right]. \tag{4}$$

Finally the definition of the root-tip loss factor is

$$f = \frac{1}{2\pi} \int_0^{2\pi} f_\psi(x, \psi) \mathrm{d}\psi, \tag{5}$$

where f_ψ is the local root-tip loss factor that includes tip and root losses, and can be expressed by

$$
\begin{aligned}
f_\psi(x, \psi) &= \left(\frac{2}{\pi}\right)^2 \arccos\left\{\exp\left[-\frac{b}{2}\frac{1-x}{x}\frac{1}{\sin\phi(x,\psi)}\right]\right\} \times \\
&\times \arccos\left\{\exp\left[-\frac{b}{2}\frac{x-x_R}{x}\frac{1}{\sin\phi(x,\psi)}\right]\right\},
\end{aligned}
$$

where b is the number of blades and x_R the is the non-dimensional position of the blade root.

Therefore, the BEMT model consists in three algebraic equations, (2), (3) and (5), that are solved to determine the three basic unknowns, that are: the azimuthal averaged axial and tangential induced factors, $a_0(x)$ and $a_0'(x)$, respectively, and the root-tip loss factor, $f(x)$. Finally, the axial induced velocity factor $a(x, \psi)$ is computed using (1) and the tangential induced velocity factor is $a'(x) = a_0'(x)$ as pointed out in [7].

2.2. Stall delay model

Stall delay or rotational augmentation has two important effects: a significant increment of the lift coefficient compared to the non-rotating case, and a delay of the angle of attack at which stall takes place. Centrifugal and Coriolis forces play a fundamental role in the behaviour of the boundary layer, especially when stall takes place close to the trailing edge of the blade. An increase of the aerodynamic drag is generally expected because the centrifugal pumping of the separated flow requires some energy, see [13]. In the last decade many authors have tried to tackle the problem of modelling stall delay and nowadays it seems there is no clear consensus on the correct way to model it, as it has been pointed out by [14] and [15]. There is an important body of literature dealing with engineering modifications of the lift and drag coefficients without rotational effects to describe stall delay and ready to be plugged into BEMT models. A comprehensive revision of these engineering models can be found in [15]. In this paper the model presented in [8] is used to take into account the stall delay phenomenon.

The lift and drag coefficients corrected to account for the stall delay phenomenon, $c_{l,3D}$ and $c_{d,3D}$, can be expressed by

$$
\begin{aligned}
c_{l,3D} &= c_{n,3D}\cos\alpha + c_{t,3D}\sin\alpha, \\
c_{d,3D} &= c_{n,3D}\sin\alpha - c_{t,3D}\cos\alpha,
\end{aligned}
$$

where the normal force and the chordwise force coefficients, $c_{n,3D}$ and $c_{t,3D}$, are related to the bidimensional normal and chordwise coefficients $c_{n,2D}$ and $c_{t,2D}$, by

$$
\begin{aligned}
c_{n,3D} &= c_{n,2D} + \int_0^1 \Delta c_p \mathrm{d}\xi, \\
c_{t,3D} &= c_{t,2D} + \int_{\eta_{LE}}^{\eta_{TE}} \Delta c_p \mathrm{d}\eta,
\end{aligned}
$$

being ξ and η the coordinates of the lower and upper airfoil surfaces, η_{LE} and η_{TE} correspond to the leading edge and to the trailing edge coordinates, respectively, and Δc_p is the difference between the actual pressure coefficient affected by rotational effects, and the pressure coefficient

measured in the wind tunnel, i.e. in bidimensional conditions. After using the model presented in [8] the following difference of pressure coefficient is proposed

$$\Delta c_p \left(\frac{c}{r}, x, \xi, \alpha, \theta\right) = \frac{2C\left(1-\xi\right)^2}{1 + \tan^2\left(\alpha + \theta\right)} \frac{c}{r} \sqrt{\frac{1+x^2}{x^2}} \left(\frac{\alpha - \alpha_{f_1}}{\alpha_{f_0} - \alpha_{f_1}}\right)^2,$$

where C is a constant, α_{f_0} and α_{f_1} are the angles of attack at which separation occurs from the leading and trailing edge, respectively.

The original work [8] provides a value of the constant $C \sim 2.5$, in order to fit the results of the NREL-UAE in the 30% of the blade span. The values of α_{f_0} and α_{f_1} have been chosen, in this case, to fit lift and drag coefficients, resulting $\alpha_{f_0} = 24$ °y $\alpha_{f_1} = 7$ °.

3. Validation of the theoretical model

As it has been mentioned in the introduction, the BEMT model used is validated against the measurements of the aerodynamic coefficients of a selected blade section and the power coefficient of the NREL-UAE wind turbine. The azimutal distributions of aerodynamic coefficients are presented in this paper only for the $x = 0.8$. This blade section has been considered the most interesting to show the validity of the BEMT model because it represents a trade-off between those sections where the agreement between experiments and computations are very good, and those others where that agreement is poorer. For instance, the constant C of the stall delay model in [8] was obtained to fit NREL-UAE results at $x = 0.3$. The application of this model to the BEMT computation leads in general to good results at the very inner sections and shows bad agreement at the tip.

Figure 1 shows the comparison between the measurements and the computations of the normal and tangential aerodynamic coefficients at the blade section $x = 0.8$ for the wind turbine of the NREL-UAE operating at $U_\infty = 15\text{m/s}$ and for two yawed conditions, $\Phi = 30°$ and $\Phi = 60°$. It can be seen that at $\Phi = 30°$, the normal coefficient, figure 1(a), shows a bad agreement with the experimental results, while the tangential coefficient, figure 1(b) exhibits a better agreement, especially for the azimuths [60°, 300°]. However, for high yaw angles, $\Phi = 60°$, the agreement between measurements and computations of both force coefficients, figures 1(c) and 1(d), is better in the azimuth range [50°, 300°].

The main validation result is shown in figure 2, where the computed values of C_P for yaw angles $\Phi = 0°$ to $60°$, every $10°$, are compared with measurements on the NREL-UAE wind turbine, for different values of the tip speed ratio, λ. The experimental data have been obtained from [16]. The power coefficient is computed as

$$C_P\left(\lambda, \theta_C; \Phi\right) = \frac{1}{2\pi} \int\limits_{0}^{2\pi} \int\limits_{x_R}^{1} \lambda \frac{\mathrm{d}C_Q}{\mathrm{d}x} \mathrm{d}x \mathrm{d}\psi,$$

where x_R is the dimensionless root cutout and $\mathrm{d}C_Q/\mathrm{d}x$ is defined in (4) and the axial velocity induced factor, $a(x, \psi)$, is used in this expression instead of $a_0(x)$. As it can be seen, the agreement between experimental and numerical results is acceptable, especially at low tip speed ratios where blade stall plays a fundamental role. The use of the stall delay model of [8] leads to a significant improvement at low tip speed ratios. In the authors' experience classical BEMT models applied to the non-yawed rotor without stall delay model compares worst to the experimental data at lower tip speed ratios, such as $\lambda < 4$, than the BEMT with a stall delay model implemented.
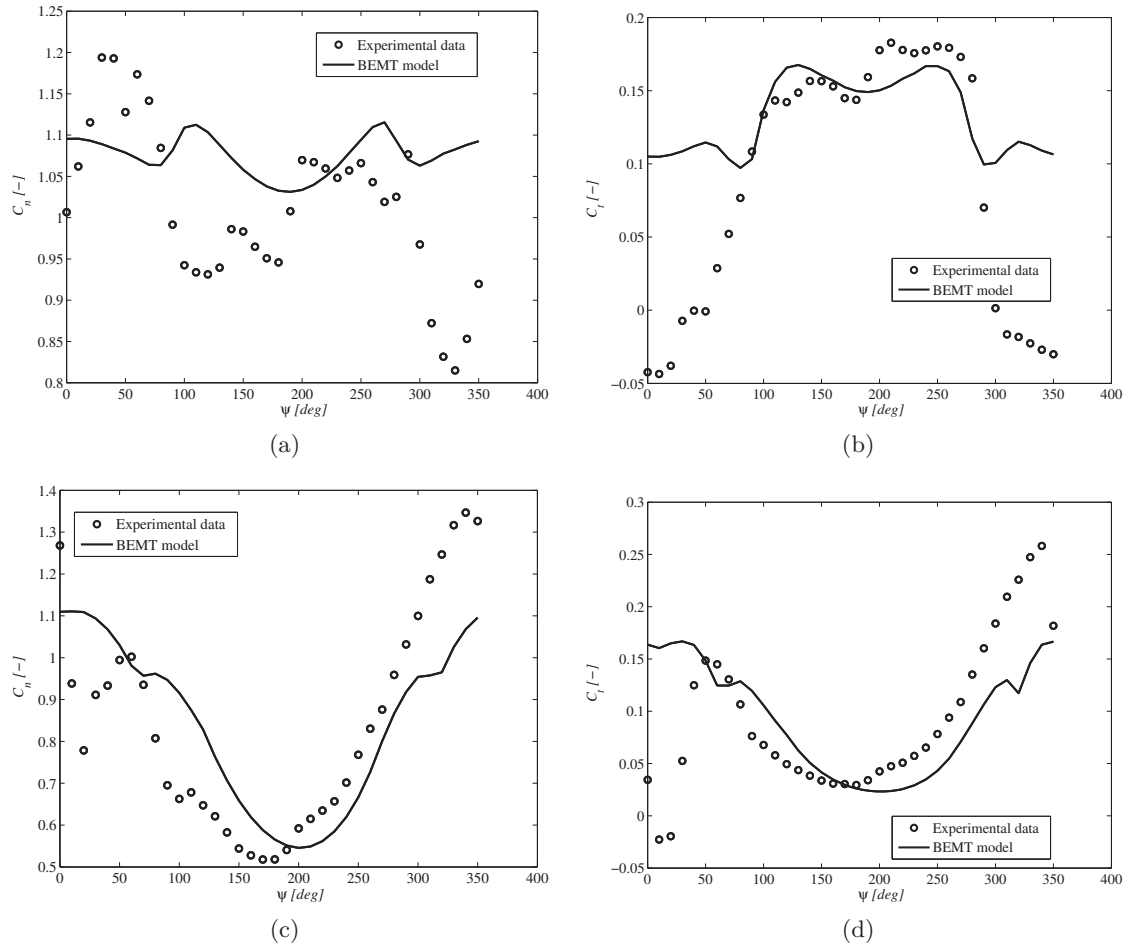
Figure 1: Comparison of distributions of aerodynamic force coefficients between NREL-UAE data and computed values for the non-dimensional blade position of $x = 0.8$ and wind speed $U_\infty = 15$ m/s. (a) Normal force coefficient, C_n, and $\Phi = 30°$ (b) tangential force coefficient C_t, and $\Phi = 30°$ (c) Normal force coefficient, C_n, and $\Phi = 60°$ (b) tangential force coefficient C_t, and $\Phi = 60°$.

4. Optimisation results in yawed conditions

The power coefficient, has been obtained as a function of the tip speed ratio, the blade control angle and, for the yawed condition, the yaw angle. This function, $C_P(\lambda, \theta_C; \Phi)$, is determined using the above described BEMT model, and the values of the tip speed ratio, $\lambda_{\mathrm{op}}(\Phi)$, and blade control angle angle, $\theta_{C\mathrm{op}}(\Phi)$, that yield maximum power coefficient for each yaw angle, Φ, are calculated using standard two variables maximisation algorithms. These optimum values are shown in figure 3 for the NREL-UAE rotor. As it can be observed in the figure, for achieving maximum power coefficient, the value of the tip speed ratio, λ, must increase as Φ increases (about one unit from $\Phi = 0°$ to $\Phi = 30°$) while the blade control angle, $\theta_{C\mathrm{op}}$, must decrease about 1.5° in the same interval of Φ.

Figure 4 shows the maximum values of C_P that can be obtained if the wind turbine is run at $\lambda_{\mathrm{op}}(\Phi)$, $\theta_{C\mathrm{op}}(\Phi)$ for each Φ, together with the maximum value of C_P if the wind turbine is operated for each yaw angle Φ with $\lambda_{\mathrm{op},0} = \lambda_{\mathrm{op}}(\Phi = 0°)$ and $\theta_{C\mathrm{op},0} = \theta_{C\mathrm{op}}(\Phi = 0°)$. In figure 4 it is also presented the recovery in $C_{P\max}$ between both control laws. It can be seen that as the
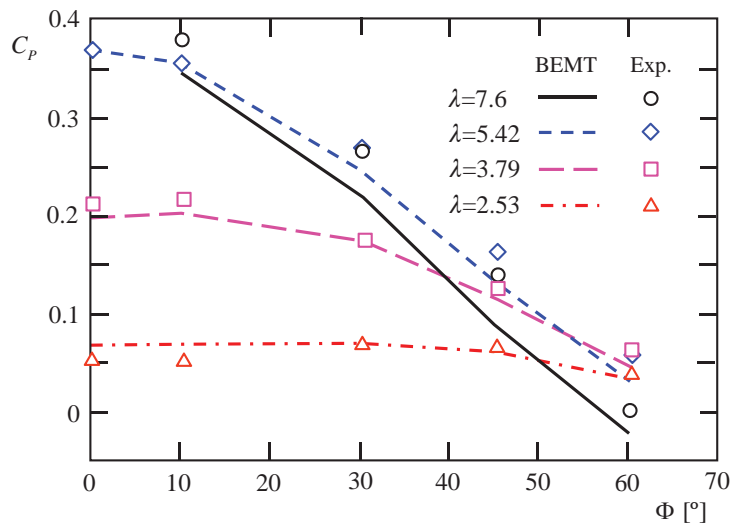
Figure 2: Power coefficient, C_P versus yaw angle, Φ, for different values of the tip speed ratio, λ. The experimental data have been obtained from [16] for the NREL-UAE experiment.
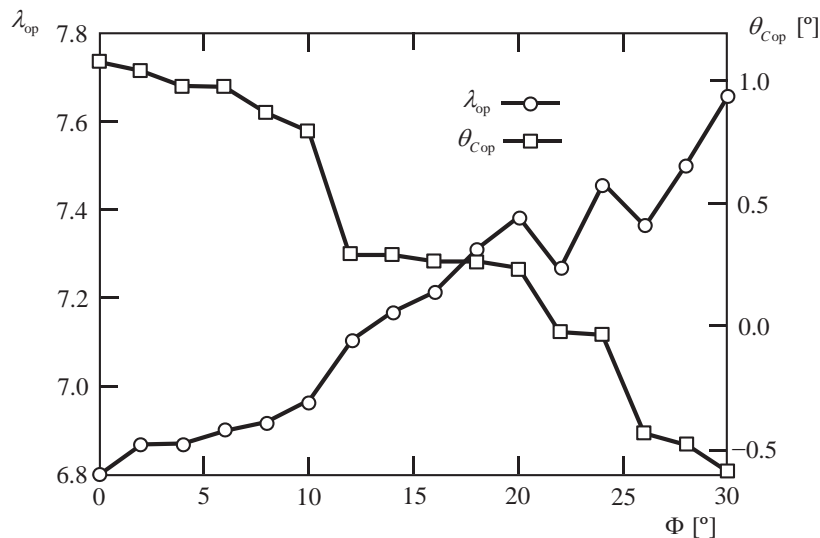

Figure 3: Optimum values for the tip speed ratio, λ_{op} and for the blade pitch angles, θ_{Cop} that maximises C_P for each yaw angle Φ.

yaw angle increases the recovery in the power coefficient increases as well, reaching a value of 10% for $\Phi = 30°$. As the yaw angle increases the effect of using the optimum laws $\lambda_{op}(\Phi)$ and $\theta_{Cop}(\Phi)$ compared to the non-yawed $\lambda_{op,0}$ and $\theta_{Cop,0}$ laws increases, leading to a larger recovery in the power coefficient (about 10% for $\Phi = 30°$).

5. Conclusions
The NREL-UAE rotor is analysed with a BEMT model in order to obtain the tip speed ratio and blade control angle which optimise the power coefficient as a function of the yaw angle. The BEMT model used includes non-uniform induced velocity factors, stall delay modelling, and Prandtl-Glauert root-tip loss correction. The BEMT model has been validated
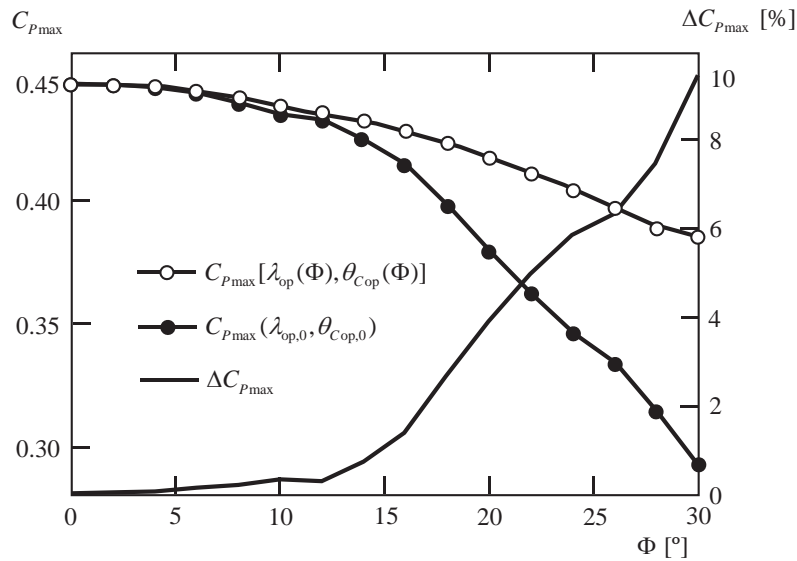
Figure 4: Maximum values of the power coefficient, $C_{P\max}$ versus yaw angle Φ, if the wind turbine is run at $\lambda_{\mathrm{op}}(\Phi), \theta_{C\mathrm{op}}(\Phi)$ for each yaw angle Φ, $C_{P\max}[\lambda_{\mathrm{op}}(\Phi), \theta_{C\mathrm{op}}(\Phi)]$; and if the wind turbine is operated for each yaw angle Φ with $\lambda_{\mathrm{op},0} = \lambda_{\mathrm{op}}(\Phi = 0°)$ and $\theta_{C\mathrm{op},0} = \theta_{C\mathrm{op}}(\Phi = 0°)$, $C_{P\max}(\lambda_{\mathrm{op},0}, \theta_{C\mathrm{op},0})$. It is also presented the gain in $C_{P\max}$ between both control laws, $\Delta C_{P\max}$.

using experimental data of the NREL-UAE. Local distribution of aerodynamic forces shows discrepancies as it can be expected. However, the values of the power coefficient for different tip speed ratios and yaw angles show a good agreement with the measurements. The use of a delayed-stall model has improved the agreement with experimental data at low speed ratios.

It has been obtained that the value of the tip speed ratio and the blade control angle must increase and decrease, respectively, to achieve maximum power coefficient as the yaw angle increases.

The authors understand that these results could be controversial, most probably they are blade dependent, and even there is a possibility that the results could be within the uncertainty margin of the BEMT model, since the required variations predicted for the tip speed and blade control angle are small. However the authors consider that the validation of the results presented, by means of more advanced computational methods or wind tunnel testing, with high resolution in the tip speed ratio and the blade control angle, would be clarifying in all aspects.

References

[1] Anderson 1979 *Multi-Science Publishing Co. Ltd.* ed Wind Energy Workshop s (April 19-20 1979, Cranfield, Beds., England) pp 57–67
[2] Divalentin E 1986 *European Wind Energy Conference, Rome* (European Wind Energy Association)
[3] Hau E 2000 *Windturbines : fundamentals, technologies : application and economics* (Berlin: Springer)
[4] Loland K 2011 Wind turbine in yawed operation Tech. Rep. EPM-M-2011-29 NTNU
[5] Imamura H, Takezaki D, Hasegawa Y, Kikuyama K and Kobayashi K 2004 *Europeand Wind Energy Conference, London* (European Wind Energy Association)
[6] Hand M, Simms D, Fingersh LJand Jager D, Schreck S and Larwood S 2001 Unsteady aerodynamics experiment phase VI: wind tunnel test configurations and available data campaigns Tech. Rep. NREL/TP-500-29955 National Renewable Enery Laboratory
[7] Burton T, Sharpe D, Jenkins N and Bossanyi E 2001 *Wind Energy Handbook* (Chichester: John Wiley and Sons)
[8] Bak C, Johansen J and Andersen P 2006 *Europeand Wind Energy Conference, Athens* (European Wind Energy Association)

[9] Chen R 1989 A Survey of Nonuniform Inflow Models for Rotorcraft Flight Dynamics and Control Applications Tech. Rep. NASA-TM-102219 National Aeronautics and Space Administration

[10] Coleman R, Feingold A and Stempin C 1945 Evaluation of the induced velocity of an idealised helicopter rotor Tech. Rep. NACA ARR L5E10 National Advisory Committee for Aeronautics

[11] Shen W, Mikkelsen R, S, Sørensen J and Bak C 2005 *Wind Energy* **8** 457–475

[12] Sant T 2007 Improving BEM-based Aerodynamic Models Tech. rep. Delf University, Wind Energy Research Institute, DUWIND

[13] Lindenburg C 2004 *Europeand Wind Energy Conference, London* (European Wind Energy Association)

[14] Simms D, Schreck S, Hand M and Fingersh L 2001 NREL Unsteady Aerodynamics Experiment in the NASA-Ames Wind Tunnel: A comparison of predictions to measurements Tech. Rep. NREL/TP-500-29494 National Renewable Enery Laboratory

[15] Breton S P, Coton F N and Moe G 2008 *Wind Energy* **11** 459–482

[16] Tongchitpakdee C, Benjanirat S and Sankar L 2005 *J. Struct. Eng.* **124** 464–474